

Article

Ultrasonic Vibration as a Primary Mixing Tool in Accelerating Aluminum–Copper Alloys Preparation from Their Pure Elements

Abdulsalam Muhrat * , Hélder Puga  and Joaquim Barbosa 

CMEMS-UMinho, Mechanical Engineering Department, University of Minho, 4800-058 Guimarães, Portugal

* Correspondence: id5666@alunos.uminho.pt; Tel.: +351-253-510220

Received: 12 June 2019; Accepted: 4 July 2019; Published: 12 July 2019



Abstract: In this study, ultrasonic vibration (USV) was evaluated in preparation of Al–8wt.%Cu alloys at a lab-scale. Moreover, the role of Ti–6Al–4V sonotrode erosion and its contribution in grain refining were analyzed. Based on the experimental conditions/parameters, it was found that the amount of impurities and the associated porosity were significantly reduced in USV treated alloys. Furthermore, USV reduced the time needed for dissolving the alloying element Cu, nevertheless, the best dissolving of Cu in this study was not possible without introducing further holding time. As a result of using a titanium-based sonotrode, a noticeable content of Ti was found in the ultrasonically treated alloys due to sonotrode erosion under USV. The dispersion of $TiAl_3$ promoted, as a main factor, a grain refining effect at relatively constant and high melt temperature, other possible mechanisms of grain refining have been discussed.

Keywords: ultrasonic vibration; aluminum alloy; impurities; porosity; grain refining; sonotrode erosion; stirring

1. Introduction

The reliability of research results highly depends on the quality of the utilized materials such as the filler alloys in brazing or welding. In many brazing or welding studies, filler alloys have to be designed and developed according to the research objective [1]. The quality of the filler alloy is the first precondition for a successful brazing process. The developing of the required lab-scale alloys could start from their pure elements [2], from master alloys and pure elements [3], or the filler alloy could be mixed during the brazing process itself by using interlayers of the alloy elements [4]. Element concentrations in the final alloys can be slightly different from the theoretical ones depending on the processing conditions of the melt.

Braze filler alloys should be free of pores and oxides, and they should have a homogeneous distribution of alloying elements. In lab-scale brazing experiments, for each type of filler alloy under testing, the quantity of filler is usually limited. Therefore, preparing a filler alloy at a lab-scale is an imperative step in several cases, since the required alloy cannot be found ready in the market nor be obtained in a small quantity. Consequently, more attention should be paid in this regard.

Concerning defects in aluminum castings, porosity has been held as the defect responsible for the majority of failures. Hydrogen and shrinkage are the main contributors to porosity formation, while the bifilms act as crack and hydrogen porosity initiators [5,6]. Hydrogen dissolves easily in liquid aluminum, but it is far less soluble in the solid state of aluminum—during solidification, the excess hydrogen is rejected from the solidification front, forming an interdendritic porosity [5,7].

Ultrasonic vibration (USV) provides multiple significant effects in melt processing. High-intensity USV generates oscillating pressure inside the melt. The formation of cavities (the tiny bubbles) occurs

under the tensile stresses during the rarefaction half period of the oscillating pressure. During a USV application in a melt, continuous formation, expansion, and collapsing of the formed bubbles take place. The bubbles collapsing is a result of the next compression half period of the oscillating pressure. On the other hand, the medium and large bubbles can coalesce and float to the surface of the melt, thus absorbing the dissolved gas. The formation of those numerous cavities and their subsequent actions promote—among other effects—the melt degassing, the wetting of solid inclusions, and microstructure modifications [8]. A high level of degassing was reported by applying USV in a molten Al–9Si–3Cu alloy for 2 min at 700 °C [9]. At a lower temperature range, the application of USV to an Al–9Si–3Cu–(Fe) alloy during cooling until 618 and 580 °C changed the morphology of primary α -Al from dendritic to a more globular structure [10]. In that study, a USV modified and homogeneously dispersed the intermetallic compounds in the matrix, compared with the non-USV-treated samples. Additionally, in many alloy systems, USV has proven to be an effective tool for grain refining and microstructure modification. For instance, the modification of AZ91 grains to globular ones [11], the refining of coarse dendrites, and the redistribution of solute elements homogeneously which can occur by applying USV during the solidification of the Ti–44Al–6Nb–1Cr alloy [12].

The effect of the alloying elements on the properties of an alloy would be valid and significant only if the homogeneous distribution of those alloying elements through the alloy is achieved. For instance, the uneven distribution of Zr, which has a low solubility in aluminum, may produce a coarse primary intermetallic in the structure where the concentration of that element is high [13]. By applying USV, the homogenization of melts could be accelerated helping to achieve a true solution state without a superheating step in shorter holding times, e.g., the USV effect reported in the Al–Pb–Na–Ca, Pb–Sn and Al–Fe alloys [8].

When adding alloying elements to molten aluminum in normal air conditions, a fast oxidation of the surfaces takes place. The oxides on the surfaces of an element being charged into the melt slow its dissolution in the matrix. On the other side, in USV applications, the surfaces of those oxidized particles in the melt act as scattering sources of the vibration and, at the same time, act as cavitation nuclei which should accelerate the dissolving of the charged element. The strong acoustic streams and secondary flows, as results of cavitation, promote the rapid mixing of the soluble and insoluble inclusions [8,14].

This work aimed to study the effect of employing USV in producing lab-scale Al–Cu alloys. The Al–8wt.%Cu alloys preparation was done without any further melt processing such as pre-settling operation, inert atmosphere, argon degassing, filtration, or fluxing [15]. In the present study, the effects of USV on the content of defects, microstructure modification, and Cu dissolving level were investigated. Furthermore, the role of sonotrode erosion in grain refining was analyzed and discussed.

2. Materials and Methods

2.1. Materials

Commercial pure aluminum cuts with similar size ranges and (30 × 30 × 2 mm³) copper segments were prepared and cleaned by detergent, hot water, and acetone before being dried thoroughly. An aluminum oxide crucible with the internal dimensions shown in Figure 1-Section A was used for the melting process. The chemical composition of the commercially pure elements (CP) is presented in Table 1.

Table 1. Composition of the pure elements in wt.%.

Element	Si	Cu	Fe	Zn	Al
CP Al	0.055	0.008	0.059	-	Bal.
CP Cu	-	Bal.	-	0.296	-

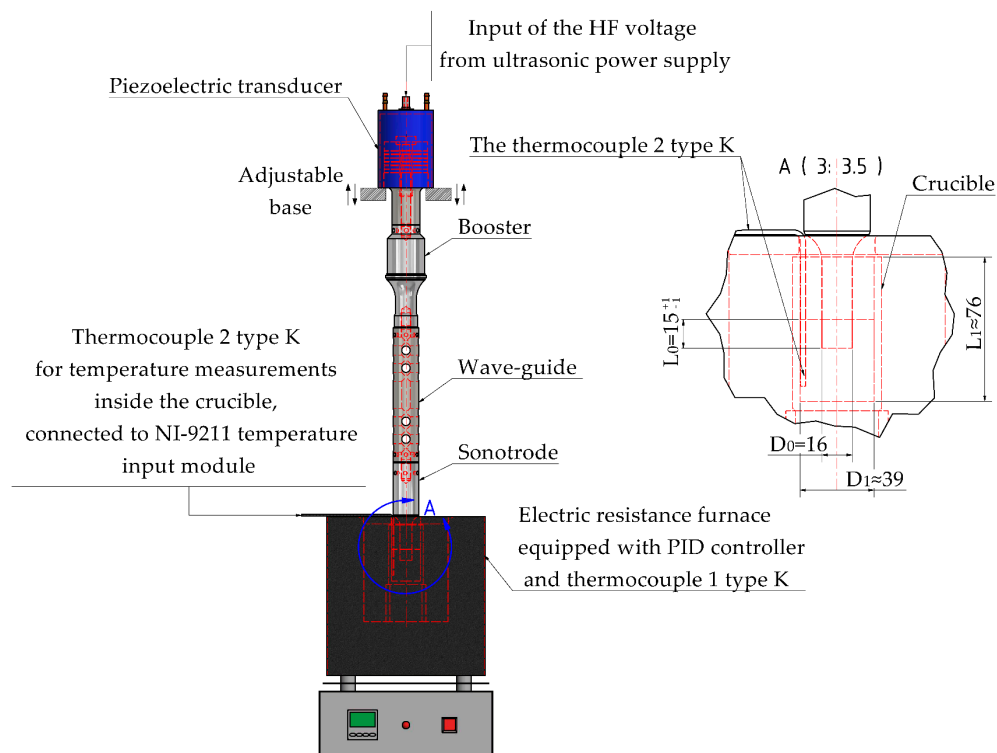


Figure 1. Schematic diagram of the ultrasonic vibration (USV) process showing the mechanical parts of the ultrasonic system, crucible dimensions (D_1 and L_1), the sonotrode tip diameter D_0 , the immersing distance D_0 of the sonotrode inside the melt, and the additional thermocouple 2 and its location for monitoring the melt temperature. All dimensions are by mm.

The most recent phase diagram of Al–Cu was given by Riani et al. [16], who based theirs on the diagram suggested by Liu et al. [17]. To carry out this study, a hypoeutectic Al–Cu alloy with a theoretical ratio of 8% Cu was chosen. The final structure of the alloy consisted of an α phase surrounded by the eutectic phase of α and $\theta(\text{Al}_2\text{Cu})$, which is stable up to 591 °C. The total weight of the melting charge was 128 ± 3 g.

2.2. Experimental Set-Up of Melt Processing

According to the total weight of the melting charge (128 ± 3 g) and the elements weight percent (Al–8Cu), the weight portions of the elements were calculated and prepared for each trial. An electrical resistance furnace equipped with a PID temperature controller was used for the melting process under normal air atmosphere. An additional two electric furnaces were used for heating the copper mold and the sonotrode. A ceramic rod was used for manual stirring. Melt temperature was acquired and recorded with a 10 readings/second acquisition-rate using a LabVIEW application, a K type thermocouple (Thermocouple 2 in Figure 1), and an NI-9211 temperature input module from National Instruments. The ultrasonic system consisted of a 1000 W ultrasonic power supply (MP Interconsulting, Le Locle, Switzerland), a high-power ultrasonic converter (piezoelectric transducer), an acoustic booster, a waveguide, and a sonotrode. Figure 1 shows a schematic diagram of the USV process including the mechanical parts of the ultrasonic system, the crucible dimensions, and the immersing distance. The sonotrode was tuned to work at 20 ± 0.2 kHz at the melt processing temperature, the delivered electrical power to the transducer was 300–330 w. The tip diameter of the manufactured sonotrode was $D_0 = 16$ mm before starting alloys preparation.

The process started at 700 ± 5 °C by adding Cu segments after Al was completely melted. After Cu addition with manual stirring using a ceramic rod, the melt was kept for 15 min, followed by additional manual stirring or USV treatments according to the selected processing method (Table 2).

The melt temperature was maintained at 700 ± 5 °C during the holding periods after mixing and between processing periods (by manual stirring or USV). After ultrasonic treatment or manual stirring and at a temperature of 695–715 °C, the melt was poured directly into a tilted copper mold under normal air atmosphere. The copper mold was pre-heated to 300 ± 5 °C and moved quickly to the casting place. An amount of the melt remained in the crucible, and it was disposed after filling the mold. Due to settling, this amount should be enriched with the inclusions/impurities of densities higher than that of the melt [18]. The surface of the melts was skimmed several times during the process and before pouring to remove dross and other floating impurities.

Table 2. Preparation parameters of the produced Al–Cu alloys.

Batch Code	Using Manual Stirring					
	Mixing	Holding	Manual Stirring	Holding	Manual Stirring	Holding
	min					
15M	5	15	2	5	-	-
45M	5	15	2	45	2	5
Batch Code	Using Ultrasonic Vibration (USV)					
	Mixing	Holding	USV	Holding	USV	-
	min					
15U	5	15	2	-	-	-
45U	5	15	2	45	2	-
90U	5	15	2	90	2	-

In the ultrasonically processed melts, the tip of the sonotrode was heated to ~ 700 °C before being transferred quickly to the melt. However, the temperature variation of the small-size treated samples during the addition/stirring/USV stages was 685–715 °C. The heated sonotrode tip caused a limited decrease in melt temperature once it was immersed to 15 ± 1 mm under the melt surface, but then the temperature started to increase up during USV and reached ~ 715 °C by the end of the process.

The solidified sample in the copper mold was removed after ~ 10 min and kept to cool down until room temperature.

The humidity and temperature were monitored and recorded using a thermo-hygrometer Testo 625 (Testo, Lenzkirch, Germany) within an hour time window during the casting process for each sample, and the average measurements for the samples in their batch are presented in Figure 2.

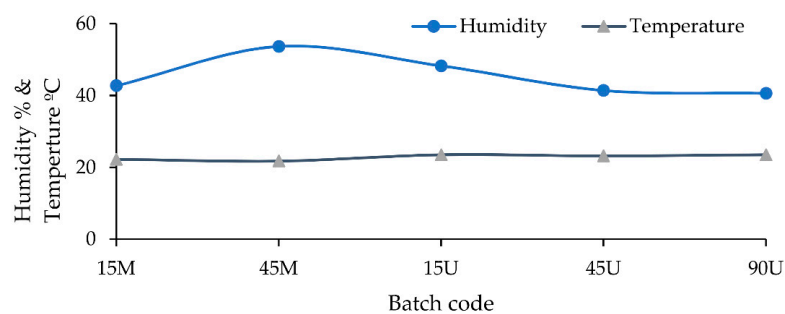


Figure 2. The average recorded humidity and temperature during the experiments.

2.3. Microstructure, Impurities, and the Associated Porosity Characterization

Samples for microstructure characterization, impurities and the associated surface porosity evaluation, and for chemical composition measurements were taken by sectioning the castings in each batch perpendicularly to their longitudinal axis, as represented in Figure 3. After cutting and polishing the section A–A of as cast-samples, the defects in the cross-section surface were evaluated and compared. Further specific analyses were conducted for the first and second phases at the same section A–A. Spectrometer analyses were performed at the cross-sections A–A and B–B.

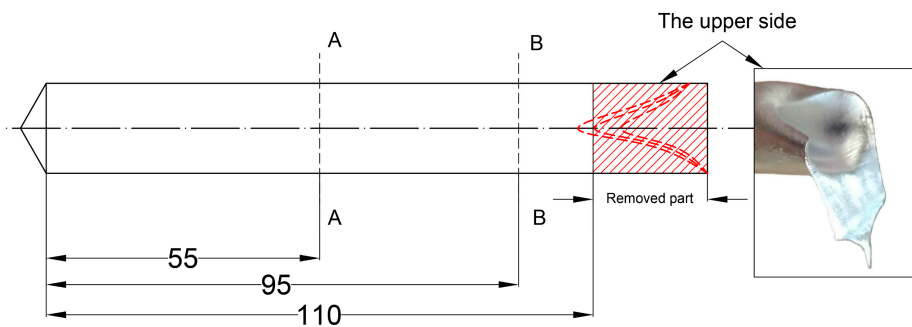


Figure 3. Schematic diagram of the as-cast sample. The examined surfaces by spectrometer were at the sections A–A and B–B, while SEM/EDS and light microscope images/analyses were taken at the section A–A. Section A–A is considered at the middle of the sample after removing the upper part. All dimensions are by mm.

The sectioned samples for microstructure, impurities and the associated surface porosity characterizations were ground using a series of increasingly finer SiC papers up to P4000 and then polished with polycrystalline 1 μm diamond suspension, followed by 0.02 μm of colloidal silica. They were then ultrasonically cleaned. The images used in evaluating the grain size and defects on the sections surfaces were obtained by a light microscope LEICA DM 2500 M (Leica Microsystems). An image processing package Fiji (ImageJ, 1.52h, National Institutes of Health, Bethesda, MD, USA) [19] were used for defects evaluation (Figure 4). The samples used for microstructure characterization by light microscope were anodized using ultrasonically stirred solution of 1.25% fluoroboric acid in distilled water. The chemical composition of the produced alloys was determined using SPECTROMAXx optical emission spectroscopy (SPECTRO, AMETEK Materials Analysis Division). For each batch of spectrometer measurements, the same standard sample with accurate composition was used for a further calibration of the measurements. A FEI Nova 200 Scanning Electron Microscope (SEM) equipped with integrated X-ray microanalysis (Energy-dispersive spectrometer EDS) was used for additional microstructure characterization and chemical composition analyses of the phases and impurities.

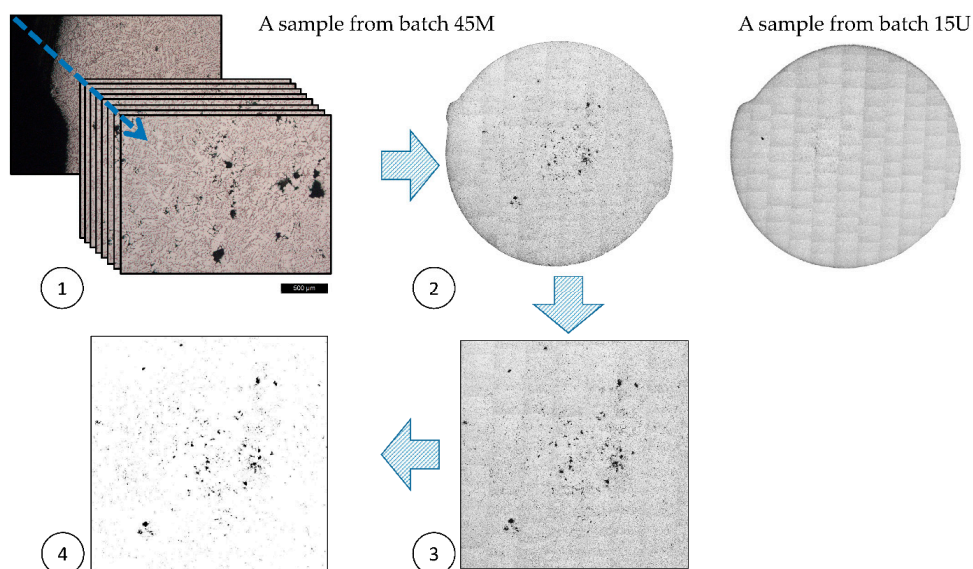


Figure 4. The followed method for calculating impurities and the associated porosity content at section A–A. (1) Obtaining microscope images for all the cross-section area at 50 \times magnification in each sample in the batch. (2) Combining and processing each sample images. (3) Extracting a central area from the combined image. (4) Processing each image by Fiji (ImageJ) software and reporting the average measurements of the samples in each batch.

At 50× magnification, a total area of $28.2 \times 28.2 \text{ mm}^2$ at section A–A in each batch was scanned and studied without chemical etching. Figure 4 demonstrates the followed method for impurities and the associated porosity characterization.

2.4. Experimental Set-Up of USV in Water

Testing USV in water with some introduced Cu segments/particles with different sizes should support the understanding of a USV application in liquid aluminum since there is some similarity with aluminum melt properties at the 700 °C temperature (close Reynolds numbers and small Ohnesorge numbers) [20]. Moreover, the acoustic spectra for liquid aluminum and water follow a similar pattern [20], which makes water the closest candidate to resemble the liquid aluminum except what concerning the attenuation [21]. Figure 5a,b shows the USV application in water with introduced Cu segments/particles which simulate the state of Cu segments in the melt after the manual mixing and partial dissolution of Cu cuts. An optimized sonotrode for work in normal temperature (slightly different length) was used for the experiment in water with similar USV parameters of the high temperature experiments in the melt. Once USV was activated, the mixture was strongly agitated. The small Cu particles distributed and circulated almost all over the water volume. Medium-sized Cu segments mostly distributed in the middle, while the largest ones were close to the cup base. Based on the experiment in water, a schematic diagram of the process in the melt of different Cu zones was suggested (Figure 5c). It is worth mentioning that the acoustic flows pattern represented in Figure 5a,c was roughly similar to the typical one presented by Eskin and Eskin [8] and Fang et al. [22].

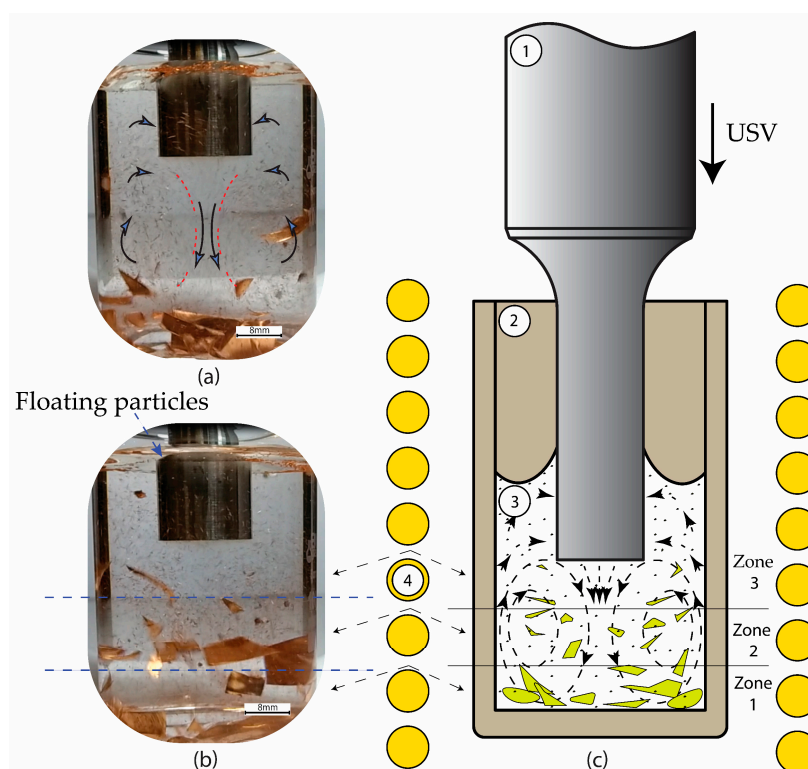


Figure 5. (a,b) USV in water with amount of Cu segments/particles. (c) Suggested schematic diagram of the USV process in the melt based on (a,b). Cu segments distributed mostly according to their sizes through Zone 1, Zone 2, and Zone 3. The relatively smaller Cu particles distribute and circulate over all the melt. 1—Sonotrode, 2—Crucible, 3—Al–Cu melt which contains unmelted amount of copper, 4—Furnace coil.

2.5. FE Optimization of the Sonotrode

A sonotrode with slightly a different length was used to apply USV in water in a normal temperature using similar USV parameters of the high temperature experiments in the melt (Figure 5). The optimization of the sonotrode dimensions, to work at 20 ± 0.2 kHz in a longitudinal vibration mode at different temperatures, was carried out using COMSOL v5.3. For the optimization at melt temperature, a linear temperature dependence to Young's modulus should be used, and the thermal expansion could be considered for further accuracy. After the preliminary design calculations and using the FEM software, the manufactured sonotrode was tested practically and readjusted to match the wanted frequency in the work temperature (Figure 6). By increasing temperature, the equilibrium interatomic separation increased, which led to a linear reduction of Young's module. The modulus E at temperature T can be described by the approximate equation [23]:

$$E = E_0 \left[1 + \alpha \left(\frac{T}{T_m} \right) \right], \quad (1)$$

where E_0 is Young's modulus at 0 K, α is the proportionality constant, and T_m is material's absolute melting temperature.

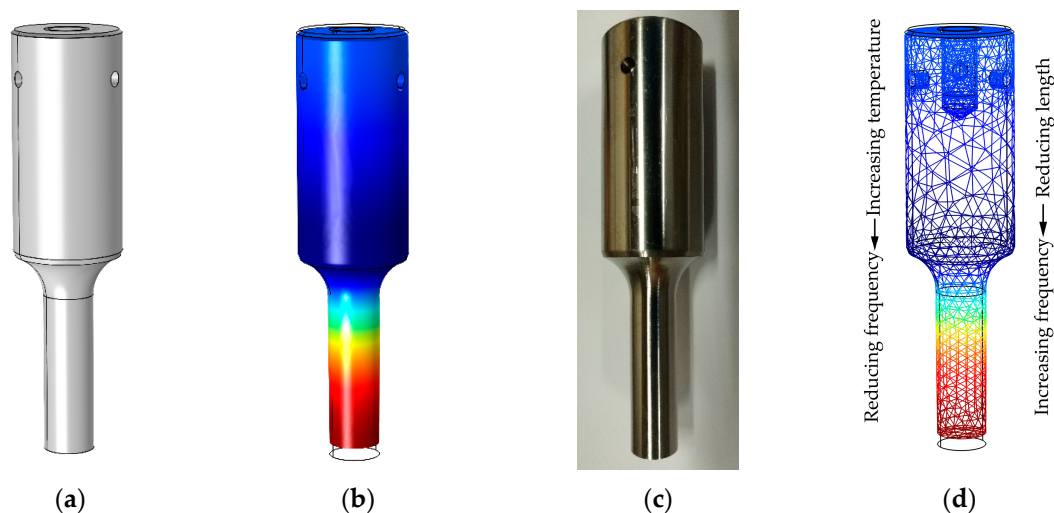


Figure 6. Optimization of the sonotrode for high temperature. (a) Sketching the main design. (b) Solving the model for a normal temperature and for a high temperature by changing the length after introducing the dependent properties on temperature (explained up); (c) manufacturing the sonotrode with some length tolerance for experimental analysis, taking into account that (d) the eigenfrequency at the wanted eigenmode (longitudinal vibration mode in the present study) can be reduced when the temperature increases and can be increased by reducing the length of the sonotrode. The attenuation factor inside the melt should be considered as well.

An analytical method was used to obtain the preliminary dimensions. The stepped sonotrode is treated as two connected cylindrical sonotrodes, and their initial design lengths—for free and unloaded stepped sonotrode at normal temperature—are an odd number of quarter-wavelength multiples [24]:

$$l_1 = (2n + 1) \frac{\pi c}{2\omega}, l_2 = (2k + 1) \frac{\pi c}{2\omega}, (k, n = 0, 1, 2, \dots), c = \sqrt{E/\rho}, \quad (2)$$

where ω is the angular frequency of vibration, c is sound speed in the rod material, and ρ is the material's density. Depending to the cross sections, correction factors could be involved in calculating l_1 and l_2 at normal temperatures [25].

The input and the output diameters can be calculated by considering the diameter of the previous part (waveguide) and the required amplification [8]:

$$k = \left(\frac{D_1}{D_2}\right)^2, \quad (3)$$

3. Results and Discussion

3.1. The Impurities and the Associated Surface Porosity Content

Following the method presented in Figure 4, the results showed that applying the first USV treatment in batch 15U resulted in substantial reduction in the defects amount at the middle section A–A of the castings, as is shown in Figure 7. In batches 45U and 90U, introducing further holding times and applying the second USV changed the observed defects content slightly, however, the measurements were more consistent comparing to batch 15U (the error bars in Figure 7).

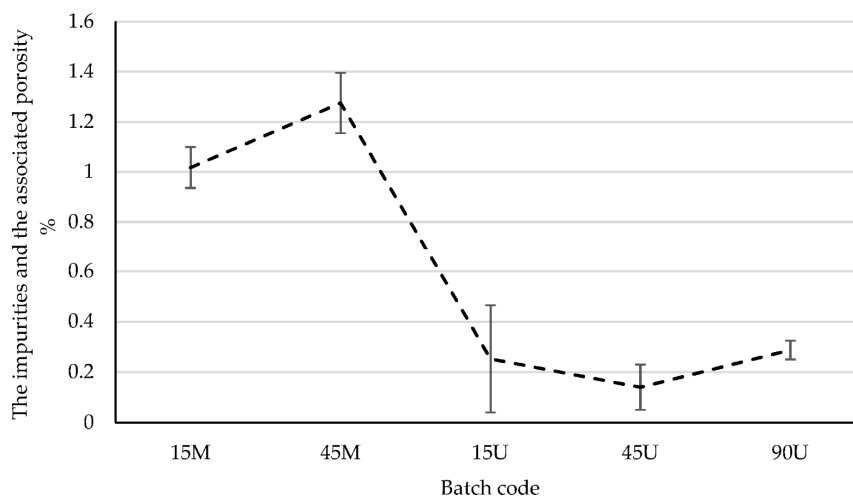


Figure 7. The content of impurities and the associated surface porosity for all batches.

After feeding Cu and applying a holding time of 15 min, the castings had many defects—mainly impurities and pores (Figure 8a). The observed quality of the samples was relatively lower after introducing a second holding time of 45 min followed by a second manual stirring period (Figures 7 and 8b). This effect was probably due to the humidity in the atmosphere, since the melt was kept for 45 min at relatively high temperature. In usual practices, many methods have been studied and applied for improving the quality of the produced alloys [15]. However, in the present study, any commercial or developed techniques were avoided in order to allow a clear understanding of USV effect on the quality of the produced alloys.

After USV treatment for 2 min, the examined cross section A–A of the samples in batch 15U showed a good section surface with reduced sizes and content of the pores (Figure 9a), compared with the manual stirred batches (Figure 8). The entire cross-sections A–A of two samples from the batches 45M and 15U are presented in Figure 4, step 2 for the comparison. In batch 45U, adding a second 2 min of USV treatment prior to casting, combined with a holding time of 45 min, produced a slightly better quality, on average. However, the produced samples had less quality variations compared with batch 15U (the error bar in Figure 7). Increasing the holding time to 90 min did not help in reducing the amount of the observed defects; inversely, the content of defects increased slightly (insignificant statistically comparing to 45U) (Figures 7 and 9c).

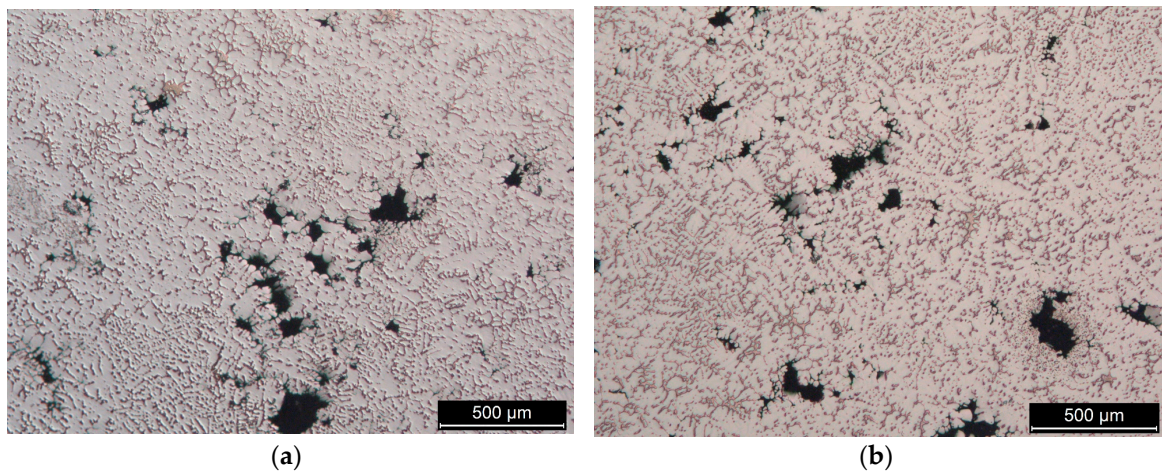


Figure 8. The produced Al-Cu alloy samples from (a) batch 15M and (b) batch 45M, both without chemical etching.

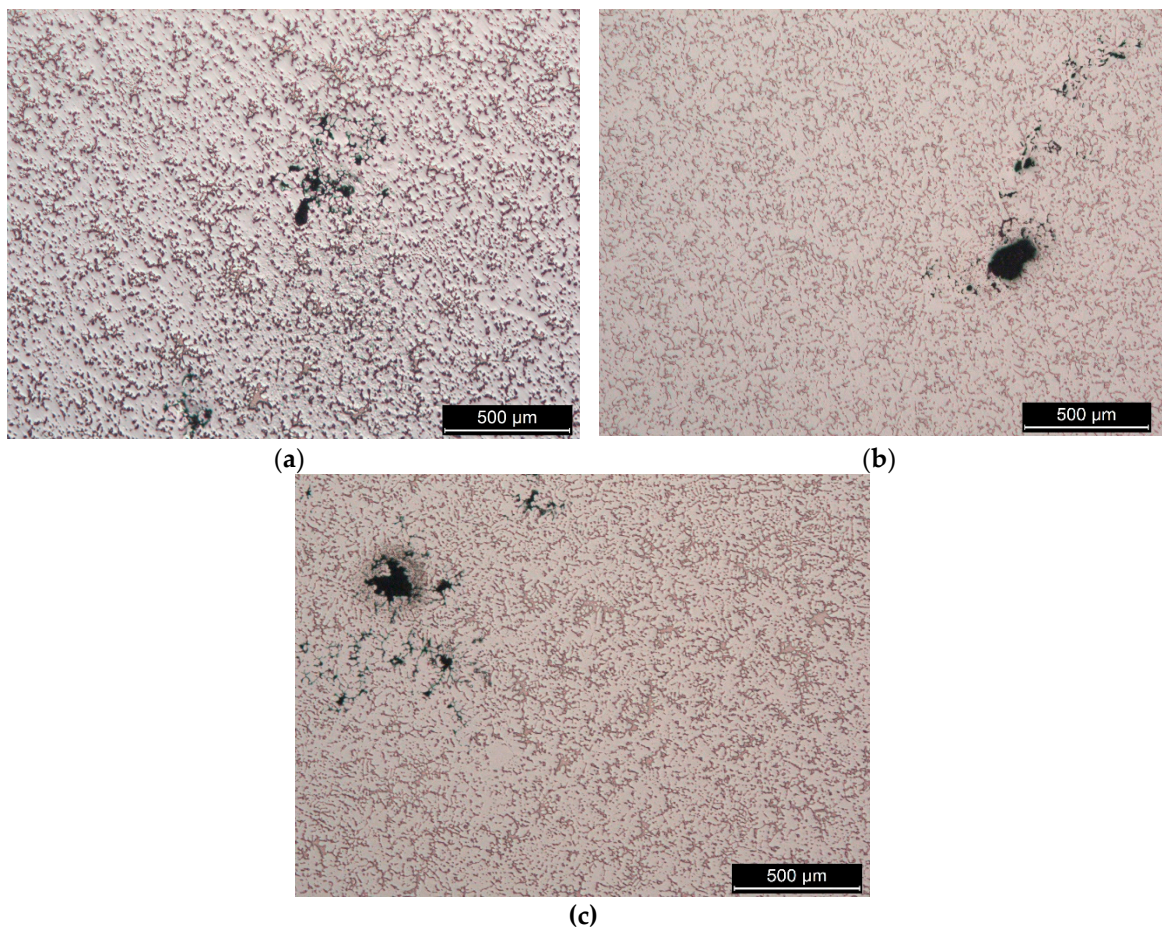


Figure 9. The produced Al-Cu alloy using USV. (a) Batch 15U, (b) batch 45U, and (c) batch 90U, all without chemical etching.

It is known that hydrogen content depends considerably on atmospheric humidity [26]. During alloy preparation and without any assistant refining or cleaning process, the alloy becomes massively contaminated with non-metallic impurities and hydrogen, such as the case of batches 15M and 45M. Applying USV was an efficient way to reduce defects in the batches 15U, 45U, and 90U (Figure 7).

The cavitation provided by USV is highly active on the surface of the impurities since their interfaces act as cavitation nuclei and favor the development of cavities [8]. According to the numerical investigation of Brujan [27], when a cavitation bubble collapses, a micro-jet is formed and reaches a high velocity between 80–120 m/s. The high-velocity micro-jet and the cyclic pressure induced by the cavities on the surface of the inclusions could initiate micro-cracking followed by the fragmentation of oxide inclusions. The acoustic streaming enhances also this effect by bringing a new melt continuously to the cavitation zone. The breakage mechanism of the titanium oxide layer under USV effect was clarified experimentally [28]. Referring to the experiment in water in the current study (Figure 5), a number of tiny particles floated to the surface of the water during USV. Based on that, after the fragmentation of inclusions, the tiniest of those particles probably moved along the cavitation bubbles and floated to the surface; this assumption is in consonance with the suggestions of Zhang et al. [29]. In general, melt processing by USV promoted the quality of the alloys by noticeably reducing the content and sizes of defects, however, the direct contribution of grain refining should be considered as well in reducing the pores sizes [30]. The grain refining is discussed in a later section.

Impurities in aluminum melts can be divided into soluble and insoluble impurities. Most of the insoluble ones are oxides from the raw materials, and other impurities come from the crucible and melting tools. The well-known fragile thin layer of oxide 10–15 μm which usually protects liquid aluminum is a main source of those oxides in the melt [31]. It should be noted that feeding Cu into the melt in normal atmosphere should be fast enough to prevent a severe oxidation of the surface if no protection method is employed. Figures 10 and 11 show examples of impurities observed in the samples.

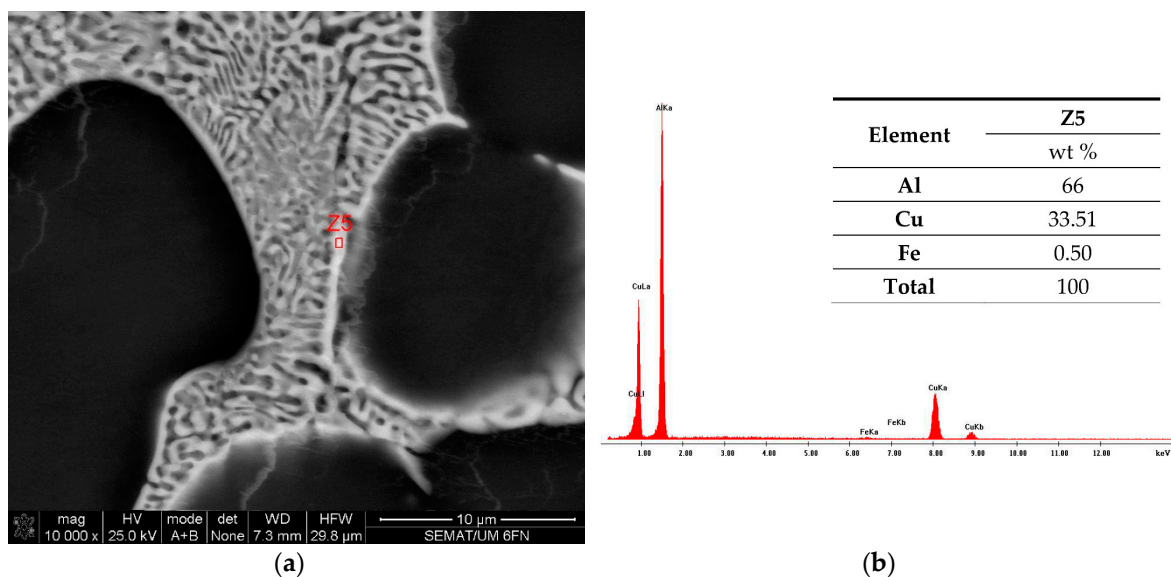


Figure 10. (a) Fe trace which appeared in few limited points in the second phase, batch 45U. (b) EDS quantification of the point in (a).

3.2. The Microstructure of the Produced Alloys

The microstructure of the produced alloys consists of typical primary α -Al dendrite surrounded by a eutectic mixture of secondary α -Al and Al_2Cu (Figure 12a,b). Figure 12c shows microscale composition variations across the eutectic and the primary phase (batch 45M).

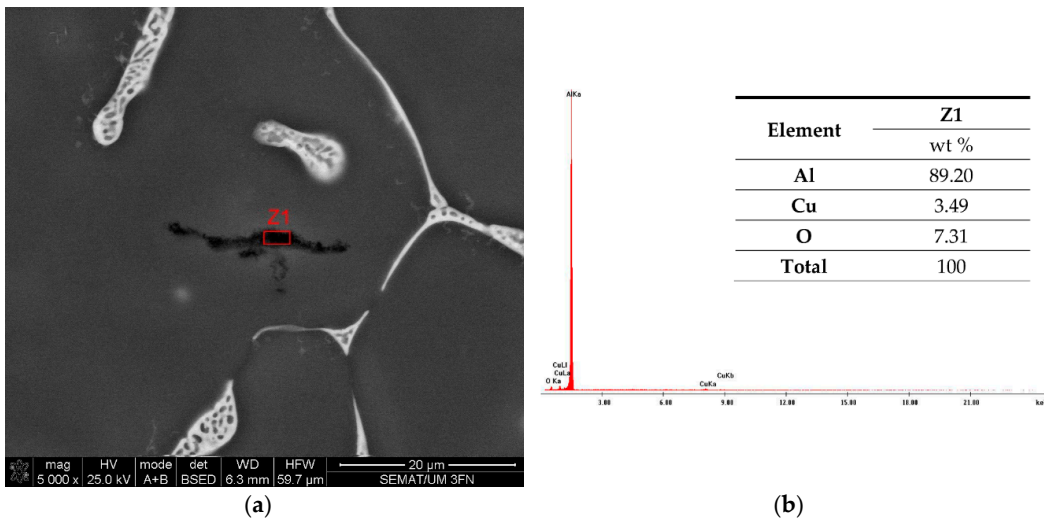


Figure 11. (a) Traces of oxides appeared in a defect location, batch 90U. (b) EDS quantification of the point in (a).

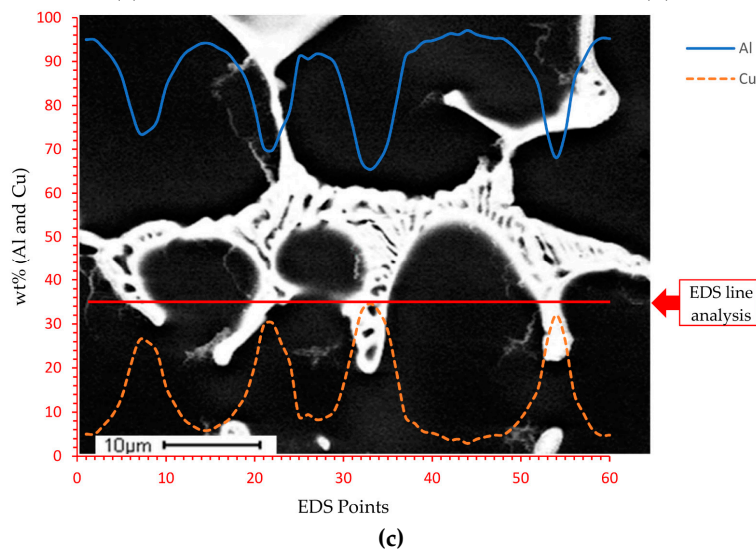
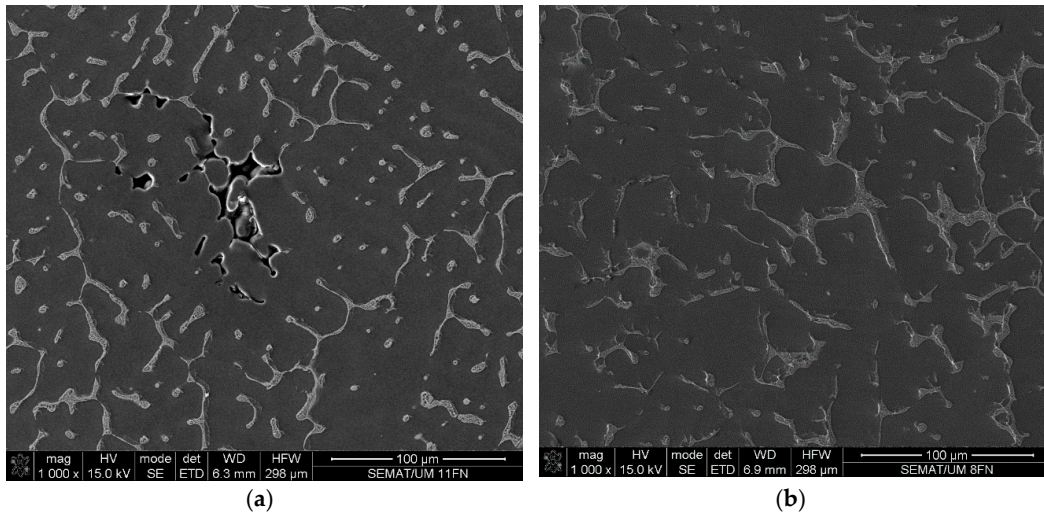


Figure 12. Microstructure of Al–Cu alloys without chemical etching (a) batch 15M and (b) batch 15U, where the lighter phase is the intermetallic Al_2Cu . (c) EDS line (60 points) showing the variation of the composition through the primary and secondary phases, batch 45M.

In the samples of batches 15U, 45U, and 90U, the heterogeneous eutectic mixture of secondary α -Al and Al_2Cu showed generally finer eutectic morphology (Figure 13c–e) in comparison to the manual stirred samples in batch 45M (Figure 13b), while the sample of batch 15M showed some irregular and finer eutectic morphology in some locations (Figure 13a) compared to batch 45M.

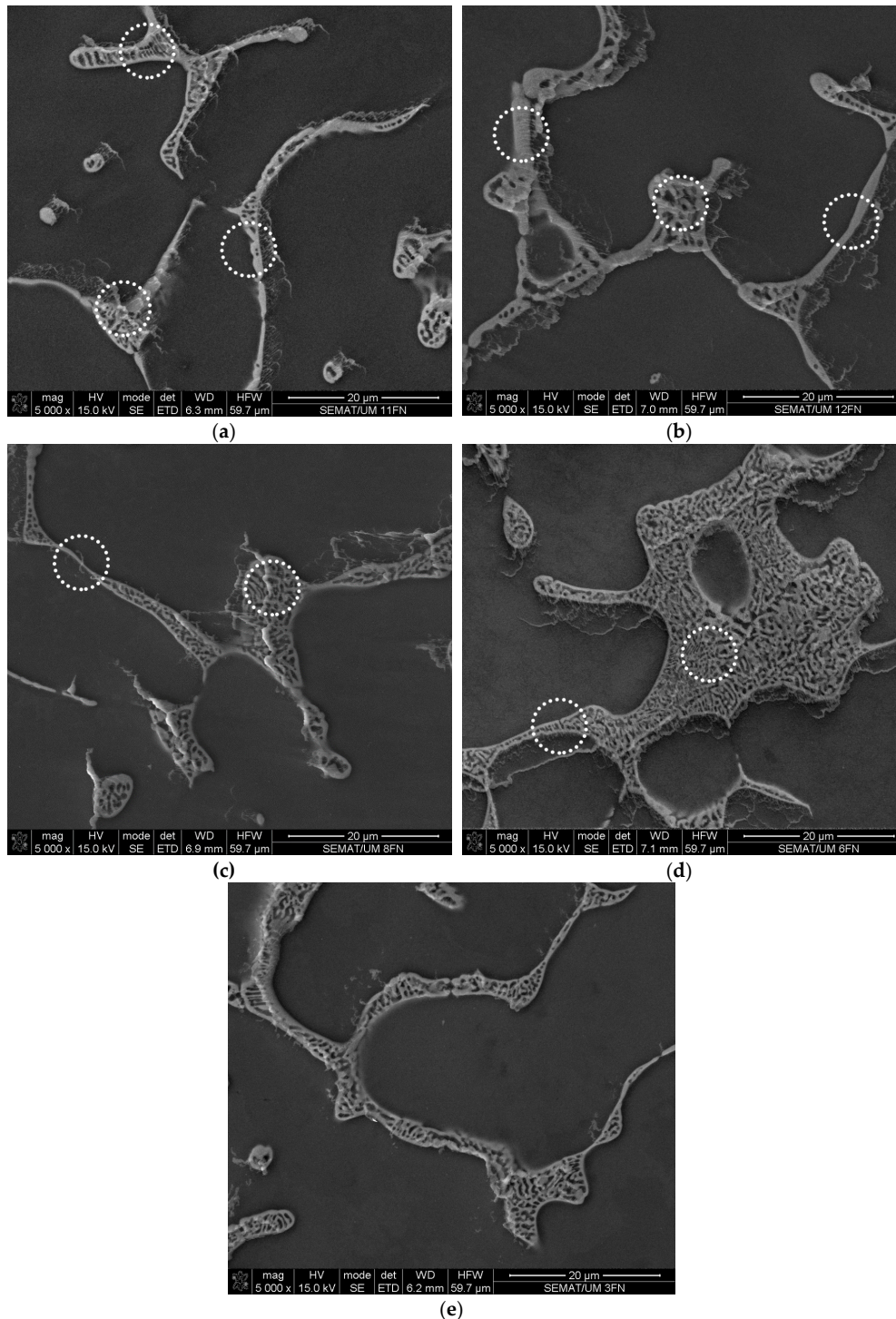


Figure 13. Microstructure of the produced alloys without chemical etching (a) batch 15M, (b) batch 45M, (c) batch 15U, (d) batch 45U, and (e) batch 90U. The USV-treated samples, as indicated the dotted circles, exhibited generally finer eutectic morphology.

The manually stirred samples exhibited normal and coarse microstructures (Figure 14a), while the samples treated by USV showed refined microstructures (Figure 14b–d). The average grain size (at 1 mm from the outer edge of section A–A) was decreased to (70–83) μm in the ultrasonically-treated alloys.

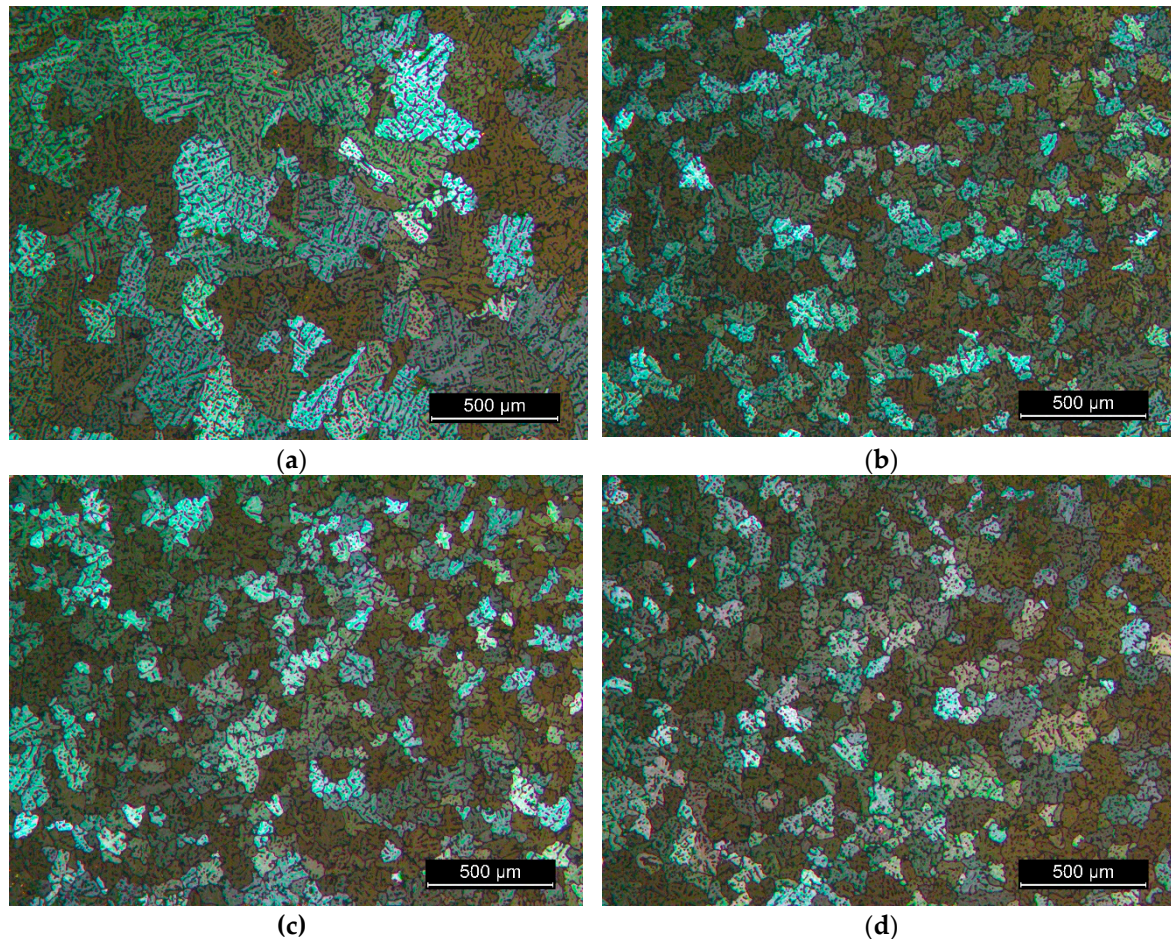
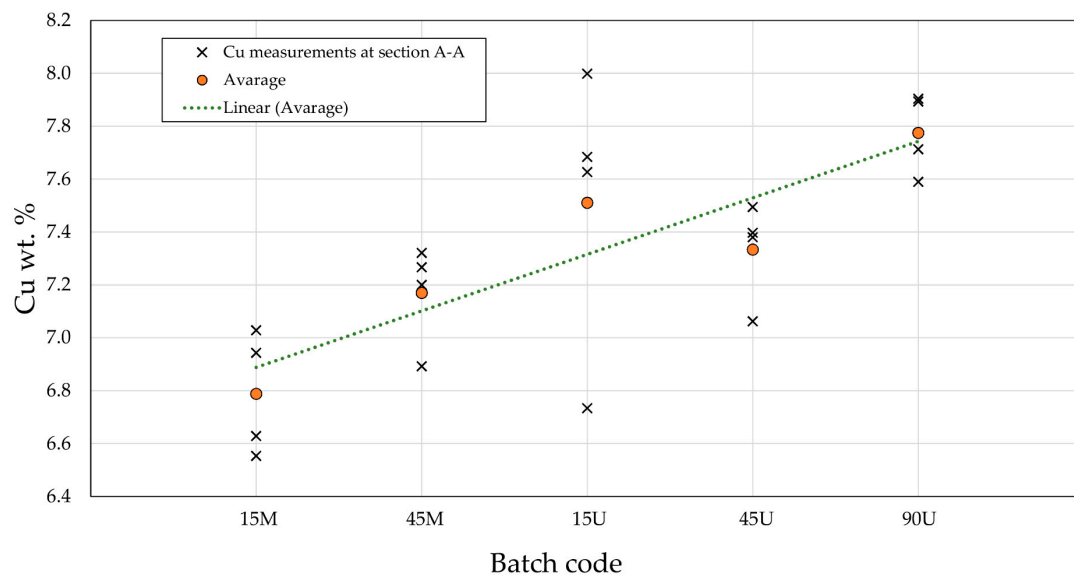


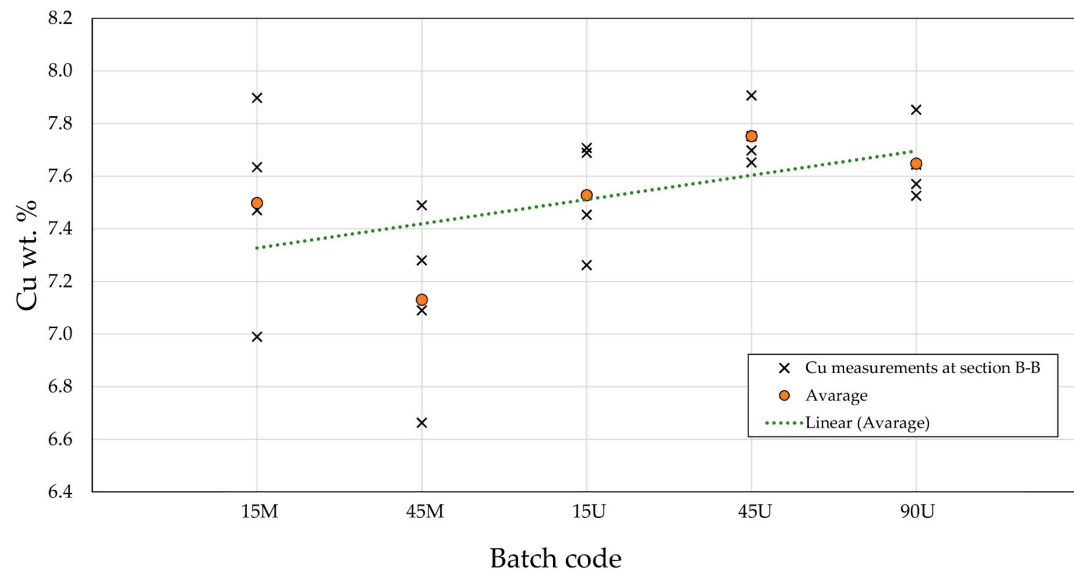
Figure 14. Microstructure of the anodized samples for grain size evaluation (a) manual stirred samples from batch 45M; USV treated ones of (b) batch 15U, (c) batch 45U, and (d) batch 90U (taken near the edge of the samples).

3.3. The Cu and Ti Content in the Produced Alloys

Optical emission spectroscopy was used to quantify the chemical composition of the produced alloys and as a macroscale indication of the alloying elements distribution. The measurements were conducted at two locations (the cross sections A–A and B–B in Figure 3), and then the measurements were calibrated by a standard sample with an accurate and known composition for greater precision. Figures 15 and 16 display the calibrated measurements and the average of Cu and Ti content, respectively, at the two specified locations. The distribution of the measurements around the mean values represents the variability in Cu% content and gives an indication of alloy homogenization over macroscale distance. Due to the USV treatment using a titanium-based sonotrode, the erosion of the sonotrode introduced an average of 0.2–0.24 wt.% of Ti in the alloys (Figure 16).



(a)



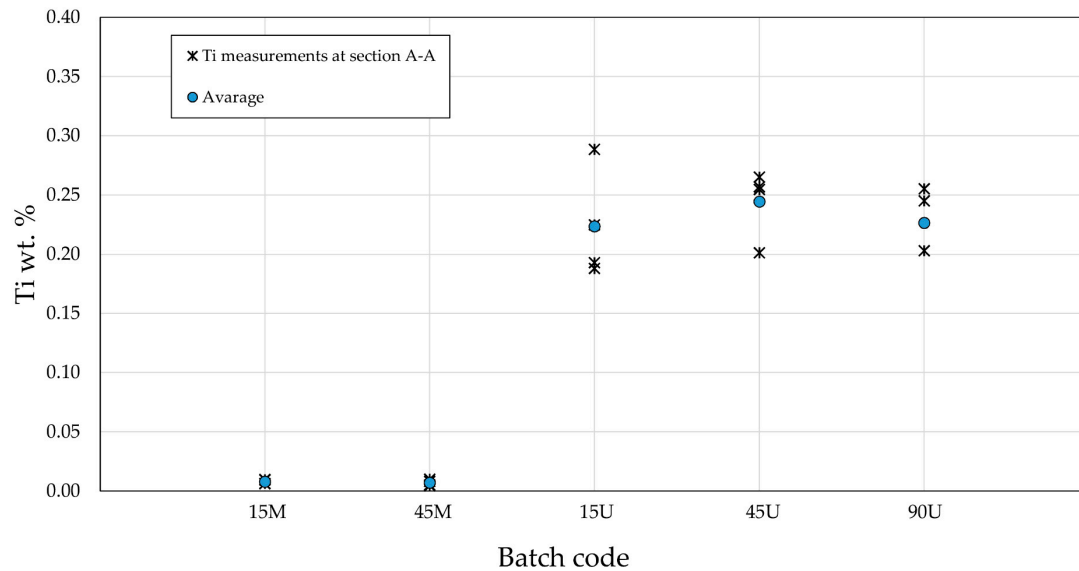
(b)

Figure 15. Cu content in the produced alloys (a) at section A–A at the middle of the samples and (b) at section B–B.

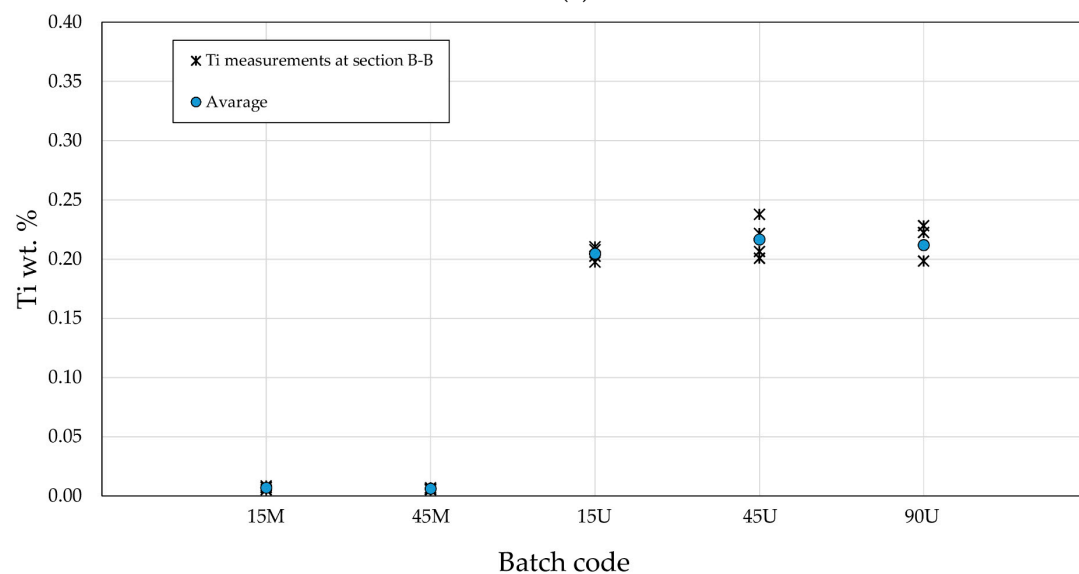
It is evident from Figure 15 that applying USV or/and increasing the holding time increases the dissolved content of copper and improves alloy homogenization. The samples of batch 90U had the maximum average Cu content at the middle section A–A (Figure 15a). Compared with 45U and 90U, the Cu measurements of the batch 15U samples showed a relatively high divergence around the average value (Figure 15a) as well as a high difference around the average value of the measured defects (Figure 7). The variation in Cu content around the average value in batch 15U at the middle section A–A (Figure 15a) implies that the complete dissolution of Cu was not achieved yet.

For the batches 15M and 45M, applying a holding time without agitating the melt strongly probably ended with settling of Cu segments/particles. Therefore, when pouring the melt, an amount of those particles can be held within the remaining melt in the crucible and may enter the mold at the end of the pouring process. This remaining melt, besides the positive segregation at the top of

castings [32], could give rise to considerable variations in the average Cu content between sections A–A and B–B and also give rise to the high divergence of Cu measurements around the average value at section B–B (Figure 15b). The Cu particle settling also may explain the relatively small variation in Cu content at the middle section A–A for the 15M and 45M samples. Furthermore, the humidity changes (Figure 2), particularly for the manual stirred samples, should also be considered.



(a)



(b)

Figure 16. Ti content in the produced alloys (a) at section A–A at the middle of the samples and (b) at section B–B.

It is well recognized that most USV effects are associated with acoustic cavitation and acoustic streaming. The collapse of cavitation bubbles is coupled by shock wave generation, microstreams, and microjets, all of which can facilitate heat, mass transfer, and an increased mixing level [33]. The acoustic streaming is a steady fluid motion resulting as a consequence of the attenuation of high-amplitude USV [22]. The observation of Cu segments/particles in water (Figure 5) demonstrated that they were passing rapidly—according to their relative sizes—through the effective zone of cavitation under

the sonotrode. The powerful acoustic streaming, therefore, had significant effect in accelerating the dissolution and the distribution of the alloying element throughout the melt volume and bringing the fresh melt into the cavitation zone under the sonotrode. In spite of that, the relatively large size segments were pushed down to the crucible base, and the rapidly circulated Cu segments were also not subject to continuous erosion by the cavitation under the sonotrode. This may emphasize the need for a certain holding time along with USV treatment.

Following Figure 5, the smaller size of Cu segments/particles, the better their circulation and distribution in water. For an aluminum melt, that may also explain some result variations regarding the samples in the same batch (in ultrasonically-treated alloys). The manual feeding and stirring at the beginning of the process could leave behind some Cu segments of various sizes, leading to unequal dissolution rates during USV and giving rise to some variations in quality.

The alloying elements usually have a lower solubility in the solid phase of the base metal. Therefore, the solutes are rejected into the liquid phase during solidification, resulting in the continuous enrichment of the liquid by solutes, leaving the primary formed solid with lower solute concentration and creating microsegregation [34]. The movements of microsegregated regions over macroscopic distances produce macrosegregation [35]. Macrosegregation is one of the major and irreversible defects in castings. The chemical analyses of the batches 45U and 90U showed more consistent Cu measurements at the same section and less variation by comparing the sections A–A and B–B (Figure 15). The lowest difference was in batch 90U (almost identical), and the macrosegregation was clearer in batch 45U.

3.4. The Role of Sonotrode Erosion

Titanium and its alloys usually show a good erosion resistance in molten aluminum. However, some alloys, such as the Nb–30Ti–20W alloy, have superior resistance [36]. The cavitation erosion of the sonotrode accelerates the formation of $TiAl_3$ on its surface followed by the dispersion of the fine $TiAl_3$ particles in the Al melt [37]. By the effect of cavitation and acoustic streaming, the fine $TiAl_3$ at the beginning of USV is supposed to dissolve faster, and the melt should be saturated with homogeneously distributed Ti. The dissolution time depends also on both the melt temperature and the size of $TiAl_3$ [38]. Under USV, the reformation of tiny $TiAl_3$ could be possible by the action of local undercooling followed the collapse of the cavities. Nevertheless, due to the continuity of sonotrode erosion, the content of Ti exceeded 0.15% (the peritectic concentration in Al–Ti phase diagram at Al side) (Figure 16). Therefore, it supposed that $TiAl_3$ was stable and acted as a nucleation site for the primary aluminum phase [38,39]. Based on that, the refining effect at a relatively constant temperature higher than the liquidus temperature was possible.

The extreme pressure when a bubble collapses during USV can undercool the liquid, thus causing nucleation. The Clapeyron equation describes the relationship between the change of the pressure and the melting temperature [40]:

$$\Delta T_M / \Delta P = T \Delta V / \Delta H, \quad (4)$$

where ΔT_M , ΔP , ΔV , and ΔH are the changes in melting temperature, pressure, volume and enthalpy, respectively; and T is the absolute temperature. Without the existence of Ti, the survival of the nucleus is difficult, since the melt of Al–8Cu was ultrasonically-treated in a temperature far from its liquidus temperature. Several studies reported a poor refining effect of USV using a sonotrode with Nb tip (no dispersion and dissolution of $TiAl_3$) in a temperature higher than the liquidus temperature of the treated alloy [41,42]. In the current study, only few bulky $TiAl_3$ particles (Figure 17) were observed in the center of some grains. Further EDS analyses were conducted, and a trace of Ti was also detected in the primary phase α -Al (Figure 18 and Table 3).

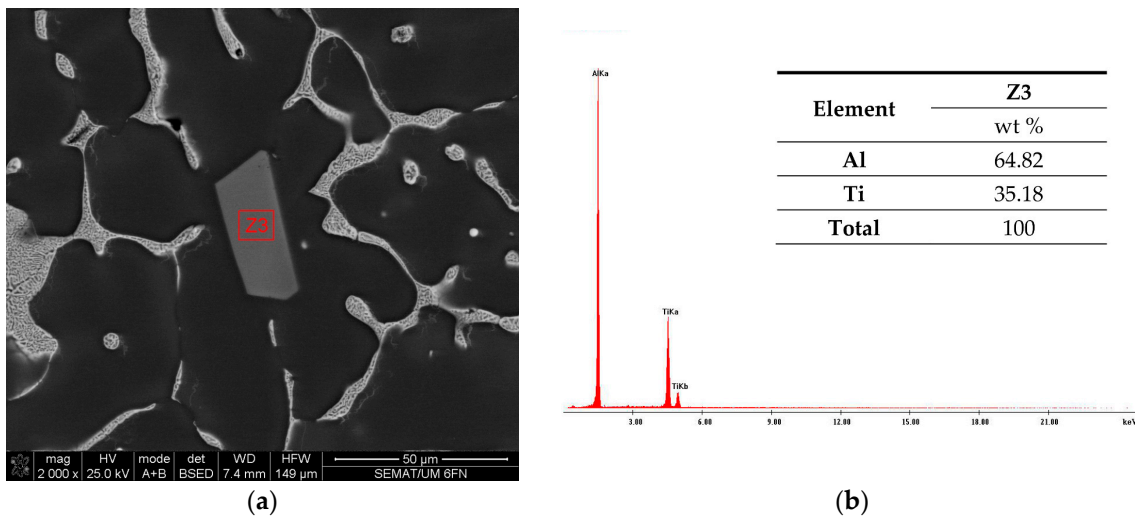


Figure 17. (a) Very few TiAl_3 particle after USV treatment, batch 45U; (b) EDS quantification of the point in (a).

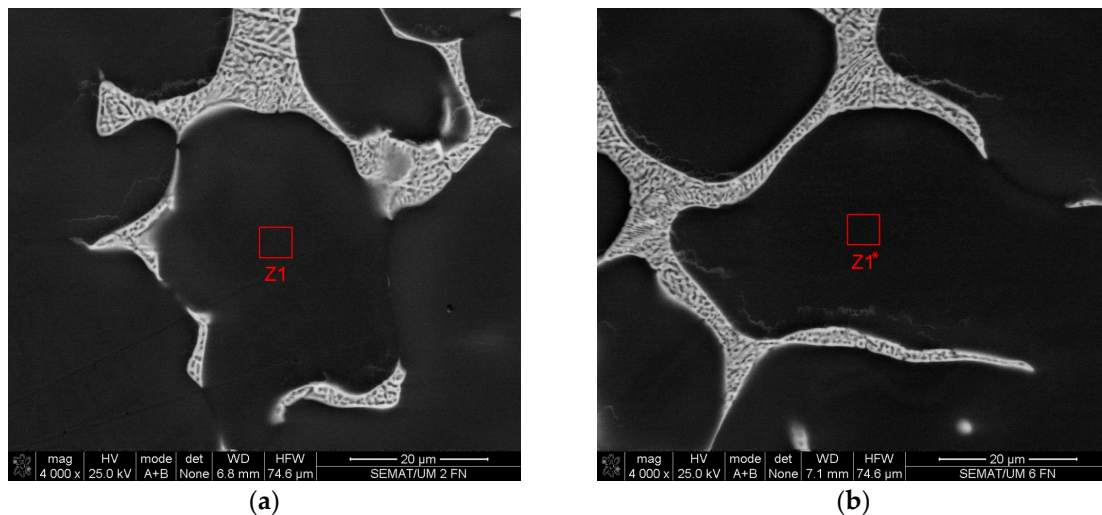


Figure 18. Traces of titanium in α -Al in (a) batch 45U and (b) batch 90U.

Table 3. EDS quantification of the points in Figure 18.

Element	Z1	Z1*
	Batch 45U	
	wt. %	
Al	96.36	96.99
Cu	2.90	2.11
Ti	0.74	0.90
Total	100	100

Other sources of heterogeneous nucleation could be considered. The wetting of non-metallic impurities' surfaces by the liquid metal becomes possible by USV, and this wetting can turn them into additional solidification sites to contribute in the grain refinement effect [43]. The nucleation behavior could be promoted by specific geometrical conditions of a microcrack on a surface of oxide where the interface between the liquid and the solid formed in the microcrack is concave. In this case, according to the Gibbs–Thomson equation, a solid embryo can exist and grow to solidification nucleus

if the temperature decreases [44]. On the other side, a Ti solute being present in the liquid can hinder the growth of Al grains [39,45,46]. According to the solute theory, the nucleants and the segregating elements are important in grain refinement. The segregating of an element and its subsequent growth restriction effects are identified by the growth restriction factor (GRF), where the local excess solute concentration ahead of the growth front causes supercooling and restricts the dendrite growth.

Though the erosion of the sonotrode is undesirable, this technique could be used for introducing fine $TiAl_3$ particles into the melt using an expendable tip of titanium or introducing any other alloying element, thus achieving a homogeneous distribution of that element.

4. Conclusions

In this study, ultrasonic vibration (USV) was employed to produce Al–8wt.%Cu alloys from their pure elements at a lab-scale. The present study analyzed and explained the effect of USV on the quality of the treated alloys, which could be regarded as a fundamental issue for further development when taking into consideration any subsequent heat treatments or filtration techniques. In addition, the impact of the Ti–6Al–4V sonotrode erosion on the microstructure was investigated. The studied effects included the content of impurities and the associated porosity, the dissolving and the distribution of the alloying element Cu, and the microstructure. The USV treatment enhanced the dissolution of copper inside the melt and improved, along with the contribution of grain refining effect, the quality of the produced alloy significantly. Nevertheless, increasing the holding time was necessary for the complete dissolution of Cu, because the Cu segments were not continuously subjected to the ultrasonic cavitation effect under the sonotrode.

The USV-treated samples showed refined grains and generally finer eutectic morphology. This study has highlighted the erosion effect of the titanium-based sonotrode on the microstructure of the treated alloy. The distribution and dissolution of fine $TiAl_3$ particles separated from the sonotrode throughout the melt were essential factors in enhancing the grain refining effect in USV treated batches at a relatively constant temperature higher than the liquidus temperature of the alloys.

Author Contributions: Conceptualization, A.M.; data curation, A.M.; formal analysis, A.M.; investigation, A.M.; methodology, A.M.; resources, A.M., H.P., and J.B.; supervision, H.P. and J.B.; validation, A.M., H.P., and J.B.; visualization, A.M.; writing—original draft, A.M.

Funding: This research received no external funding.

Acknowledgments: This work is supported by Erasmus Mundus through PEACE II Lot 2 Project 2013-2443/001-001-EMA2 and FCT with the reference project UID/EEA/04436/2013, COMPETE 2020, with the code POCI-01-0145-FEDER-006941.

Conflicts of Interest: The authors declare no conflict of interest.

References

1. Muhrat, A.; Puga, H.; Barbosa, J. Low-Temperature Brazing of Titanium Using Al-Based Filler Alloys. *Adv. Mater. Sci. Eng.* **2018**, *2018*, 1–16. [[CrossRef](#)]
2. Takemoto, T.; Okamoto, I. Intermetallic compounds formed during brazing of titanium with aluminium filler metals. *J. Mater. Sci.* **1988**, *23*, 1301–1308. [[CrossRef](#)]
3. Chen, X.; Xie, R.; Lai, Z.; Liu, L.; Zou, G.; Yan, J. Ultrasonic-assisted brazing of Al–Ti dissimilar alloy by a filler metal with a large semi-solid temperature range. *Mater. Des.* **2016**, *95*, 296–305. [[CrossRef](#)]
4. Winiowski, A.; Majewski, D. Brazing of Titanium with Aluminium Alloys. *Arch. Metall. Mater.* **2017**, *62*, 763–770. [[CrossRef](#)]
5. Dispinar, D.; Campbell, J. Critical assessment of reduced pressure test. Part 1: Porosity phenomena. *Int. J. Cast Met. Res.* **2004**, *17*, 280–286. [[CrossRef](#)]
6. El-Sayed, M.A.; Hassanin, H.; Essa, K. Bifilm defects and porosity in Al cast alloys. *Int. J. Adv. Manuf. Technol.* **2016**, *86*, 1173–1179. [[CrossRef](#)]
7. Pehlke, R.D. Formation of Porosity During Solidification of Cast Metals. In *Foundry Processes*; Katz, S., Landefeld, C.F., Eds.; Springer: Boston, MA, USA, 1988; pp. 427–445. ISBN 978-1-4612-8292-1.

8. Eskin, G.I.; Eskin, D.G. *Ultrasonic Treatment of Light Alloy Melts*, 2th ed.; CRC Press: Florida, FL, USA, 2014.
9. Puga, H.; Barbosa, J.; Gabriel, J.; Seabra, E.; Ribeiro, S.; Prokic, M. Evaluation of ultrasonic aluminium degassing by piezoelectric sensor. *J. Mater. Process. Technol.* **2011**, *211*, 1026–1033. [[CrossRef](#)]
10. Barbosa, J.; Puga, H.; Oliveira, J.; Ribeiro, S.; Prokic, M. Physical modification of intermetallic phases in Al–Si–Cu alloys. *Mater. Chem. Phys.* **2014**, *148*, 1163–1170. [[CrossRef](#)]
11. Gao, D.; Li, Z.; Han, Q.; Zhai, Q. Effect of ultrasonic power on microstructure and mechanical properties of AZ91 alloy. *Mater. Sci. Eng. A* **2009**, *502*, 2–5. [[CrossRef](#)]
12. Zheng, D.; Chen, R.; Ma, T.; Ding, H.; Su, Y.; Guo, J.; Fu, H. Microstructure modification and mechanical performances enhancement of Ti44Al6Nb1Cr alloy by ultrasound treatment. *J. Alloy. Compd.* **2017**, *710*, 409–417. [[CrossRef](#)]
13. Eskin, G.I.; Makarov, G.S.; Pimenov, Y.P. Effect of ultrasonic processing of molten metal on structure formation and improvement of properties of high-strength Al–Zn–Mg–Cu–Zr alloys. *Adv. Perform. Mater.* **1995**, *2*, 43–50. [[CrossRef](#)]
14. Eskin, G.I. Principles of ultrasonic treatment: Application for light alloys melts. *Adv. Perform. Mater.* **1997**, *4*, 223–232. [[CrossRef](#)]
15. Friedrich, B.; Kräutlein, C.; Krone, K. Melt Treatment of Copper and Aluminium—The Complex Step Before Casting. In *Continuous Casting*; Müller, H.R., Ed.; Wiley-VCH Verlag GmbH & Co. KGaA: Weinheim, Germany, 2006; pp. 1–22. ISBN 978-3-527-60796-9.
16. Riani, P.; Arrighi, L.; Marazza, R.; Mazzone, D.; Zanichchi, G.; Ferro, R. Ternary Rare-Earth Aluminum Systems with Copper: A Review and a Contribution to Their Assessment. *J. Phase Equilibria Diffus.* **2004**, *25*, 22–52. [[CrossRef](#)]
17. Liu, X.J.; Ohnuma, I.; Kainuma, R.; Ishida, K. Phase equilibria in the Cu-rich portion of the Cu–Al binary system. *J. Alloy. Compd.* **1998**, *264*, 201–208. [[CrossRef](#)]
18. Instone, S.; Buchholz, A.; Gruen, G.U. Inclusion Transport Phenomena in Casting Furnaces. *TMS Miner. Met. Mater. Soc. Light Met.* **2008**, *2008*, 811.
19. Schindelin, J.; Arganda-Carreras, I.; Frise, E.; Kaynig, V.; Longair, M.; Pietzsch, T.; Preibisch, S.; Rueden, C.; Saalfeld, S.; Schmid, B.; et al. Fiji: An open-source platform for biological-image analysis. *Nat. Methods* **2012**, *9*, 676. [[CrossRef](#)] [[PubMed](#)]
20. Tzanakis, I.; Lebon, G.S.B.; Eskin, D.G.; Pericleous, K.A. Characterizing the cavitation development and acoustic spectrum in various liquids. *Ultrason. Sonochem.* **2017**, *34*, 651–662. [[CrossRef](#)] [[PubMed](#)]
21. Tzanakis, I.; Lebon, G.S.B.; Eskin, D.G.; Pericleous, K.A. Characterisation of the ultrasonic acoustic spectrum and pressure field in aluminium melt with an advanced cavitometer. *J. Mater. Process. Technol.* **2016**, *229*, 582–586. [[CrossRef](#)]
22. Fang, Y.; Yamamoto, T.; Komarov, S. Cavitation and acoustic streaming generated by different sonotrode tips. *Ultrason. Sonochem.* **2018**, *48*, 79–87. [[CrossRef](#)]
23. Courtney, T.H. *Mechanical Behavior of Materials*; Waveland Press: Long Grove, IL, USA, 2005.
24. Astashev, V.K.; Babitsky, V.I.; Khusnutdinova, K. *Ultrasonic Processes and Machines: Dynamics, Control and Applications*; Foundations of Engineering Mechanics; Springer: Berlin, Germany, 2007; ISBN 978-3-540-72060-7.
25. Grabalosa, J.; Ferrer, I.; Martínez-Romero, O.; Elías-Zúñiga, A.; Plantá, X.; Rivillas, F. Assessing a stepped sonotrode in ultrasonic molding technology. *J. Mater. Process. Technol.* **2016**, *229*, 687–696. [[CrossRef](#)]
26. Xu, H.; Jian, X.; Meek, T.T.; Han, Q. Degassing of molten aluminum A356 alloy using ultrasonic vibration. *Mater. Lett.* **2004**, *58*, 3669–3673. [[CrossRef](#)]
27. Brujan, E.A. Jets from pulsed-ultrasound-induced cavitation bubbles near a rigid boundary. *J. Phys. Appl. Phys.* **2017**, *50*, 215302. [[CrossRef](#)]
28. Chen, X.; Yan, J.; Ren, S.; Wei, J.; Wang, Q. Microstructure and mechanical properties of Ti–6Al–4V/Al1060 joints by ultrasonic-assisted brazing in air. *Mater. Lett.* **2013**, *95*, 197–200. [[CrossRef](#)]
29. Zhang, Y.; Li, R.; Li, X.; Yang, Y.; Chen, P.; Dong, F.; Jiang, R. Possible Effects and Mechanisms of Ultrasonic Cavitation on Oxide Inclusions during Direct-Chill Casting of an Al Alloy. *Metals* **2018**, *8*, 814. [[CrossRef](#)]
30. Samuel, A.M.; Samuel, F.H. Effect of melt treatment, solidification conditions and porosity level on the tensile properties of 319.2 endchill aluminium castings. *J. Mater. Sci.* **1995**, *30*, 4823–4833.
31. Mirgaux, O.; Bellot, J.; Waz, E.; Ablitzer, D. Aluminium Flotation in Stirred Reactor: A Mathematical Model and a Computer Simulation Coupling CFD and Population Balance. *Light Metals* **2009**, *2009*, 7.

32. Ludwig, A.; Wu, M.; Kharicha, A. On Macrosegregation. *Metall. Mater. Trans. A* **2015**, *46*, 4854–4867. [[CrossRef](#)]
33. Leong, T.; Ashokkumar, M.; Kentish, S. The fundamentals of power ultrasound—A review. *Acoust. Aust.* **2001**, *39*, 10.
34. Beckermann, C. Macrosegregation. *Encycl. Mater. Sci. Technol.* **2001**, *47*, 4733–4739.
35. Ghosh, A. Segregation in cast products. *Sadhana* **2001**, *26*, 5–24. [[CrossRef](#)]
36. Yan, M.; Fan, Z. Review Durability of materials in molten aluminum alloys. *J. Mater. Sci.* **2001**, *36*, 285–295. [[CrossRef](#)]
37. Dong, F.; Li, X.; Zhang, L.; Ma, L.; Li, R. Cavitation erosion mechanism of titanium alloy radiation rods in aluminum melt. *Ultrason. Sonochem.* **2016**, *31*, 150–156. [[CrossRef](#)] [[PubMed](#)]
38. Easton, M.; StJohn, D. Grain refinement of aluminum alloys: Part I. the nucleant and solute paradigms—a review of the literature. *Metall. Mater. Trans. A* **1999**, *30*, 1613–1623. [[CrossRef](#)]
39. Kashyap, K.T.; Chandrashekar, T. Effects and mechanisms of grain refinement in aluminium alloys. *Bull. Mater. Sci.* **2001**, *24*, 345–353. [[CrossRef](#)]
40. Hunt, J.D.; Jackson, K.A. Nucleation of Solid in an Undercooled Liquid by Cavitation. *J. Appl. Phys.* **1966**, *37*, 254–257. [[CrossRef](#)]
41. Alba-Baena, N.; Pabel, T.; Villa-Sierra, N.; Eskin, D.G. Effect of Ultrasonic Melt Treatment on Degassing and Structure of Aluminium Alloys. *Mater. Sci. Forum* **2013**, *765*, 271–275. [[CrossRef](#)]
42. Atamanenko, T.V.; Eskin, D.G.; Zhang, L.; Katgerman, L. Criteria of Grain Refinement Induced by Ultrasonic Melt Treatment of Aluminum Alloys Containing Zr and Ti. *Metall. Mater. Trans. A* **2010**, *41*, 2056–2066. [[CrossRef](#)]
43. Eskin, G.I. Broad prospects for commercial application of the ultrasonic (cavitation) melt treatment of light alloys. *Ultrason. Sonochem.* **2001**, *8*, 319–325. [[CrossRef](#)]
44. Dantzig, J.A.; Rappaz, M. *Solidification; 2nd Edition—Revised & Expanded*; Engineering Sciences; EPFL Press: Lausanne, Switzerland, 2016; ISBN 978-2-940222-97-1.
45. Babu, N.K.; Dayou, P.; Zheng, S.; Jun, W.; Talari, M.K. Influence of Titanium-Boron Additions on Grain Refinement of AA2219 Gas Tungsten Arc Welds. In *Light Metals 2012*; Springer: Cham, Switzerland, 2012; pp. 487–491.
46. Rohatgi, S.; Tiwari, M.; Rathi, A.; Sharma, A. Solute Particles on Grain Refinement of. *Indian Foundry J.* **2015**, *61*, 7.



© 2019 by the authors. Licensee MDPI, Basel, Switzerland. This article is an open access article distributed under the terms and conditions of the Creative Commons Attribution (CC BY) license (<http://creativecommons.org/licenses/by/4.0/>).